Fusion and direct reactions for the system 6He + 64Zn at and below the Coulomb barrier

Scuderi, V.; Di Pietro, A.; Figuera, P.; Fisichella, M.; Amorini, F.; Angulo, C.; Cardella, G.; Casarejos, E.; Lattuada, M.; Milin, Matko; ...

Source / Izvornik: **Physical Review C - Nuclear Physics, 2011, 84**

Journal article, Published version
Rad u časopisu, Objavljena verzija rada (izdavačev PDF)

https://doi.org/10.1103/PhysRevC.84.064604

Permanent link / Trajna poveznica: https://urn.nsk.hr/urn:nbn:hr:217:138069

Fusion and direct reactions for the system ^{6}He + ^{64}Zn at and below the Coulomb barrier

V. Scuderi,[1,2] A. Di Pietro,[2] P. Figuera,[2] M. Fisichella,[2] F. Amorini,[1,2] C. Angulo,[3,*] G. Cardella,[2] E. Casarejos,[3,†] M. Lattuada,[1,2] M. Milin,[5] A. Musumarra,[2,4] M. Papa,[2] M. G. Pellegriti,[1,2] R. Raabe,[6] F. Rizzo,[1,2] N. Skukan,[7] D. Torresi,[1,2] and M. Zadro[7]

[1]*Dipartimento di Fisica e Astronomia, Universitá degli Studi di Catania, 62, Via S. Sofia, I-95123 Catania, Italy*
[2]*INFN–Laboratori Nazionali del Sud and Sezione di Catania, 64, Via S. Sofia, I-95123 Catania, Italy*
[3]*CRC Louvain la Neuve, Belgium*
[4]*Dipartimento di Metodologie Fisiche e Chimiche per l'Ingegneria, Universitá di Catania, Catania, Italy*
[5]*Department of Physiscs, Faculty of Science, University of Zagreb, Zagreb, Croatia*
[6]*Instituut voor Kern-en Stralingsfysica Katholieke Universiteit Leuven, Leuven, Belgium*
[7]*Division of Experimental Physics Ruder Bošković Institute, Zagreb, Croatia*

(Received 4 November 2011; published 13 December 2011)

Fusion and transfer + breakup channels have been studied in the collision induced by the two-neutron-halo ^{6}He on a ^{64}Zn target at energies from below to above the Coulomb barrier. For comparison, the reaction induced by the stable isotope ^{4}He on the same target has been studied. The fusion cross section has been measured by using an activation technique, detecting off-line the delayed x-ray activity following the electron capture decay of the evaporation residues. New measurements of the ^{4}He + ^{64}Zn fusion cross section at sub-barrier energies have been performed in order to cover the same energy range of the ^{6}He + ^{64}Zn fusion cross section and to compare the excitation functions for the two systems down to the lowest energy data point measured for ^{6}He. From the new comparison a sub-barrier fusion enhancement has been observed in the ^{6}He case with respect to the ^{4}He one whereas no effect on the ^{6}He fusion cross section has been seen at energies above the barrier. It has been concluded that such enhancement seems to be due to the diffuse halo structure properties of the ^{6}He nucleus. Moreover, the reactions induced by ^{6}He have shown a strong yield of α particles coming from direct processes.

DOI: 10.1103/PhysRevC.84.064604 PACS number(s): 25.60.Pj, 24.50.+g

I. INTRODUCTION

The possibility of performing experiments with postaccelerated radioactive ion beams allows us to investigate new effects on the reaction mechanisms due to the peculiar structure of nuclei far from the stability valley. Typical binding energies of light neutron-rich nuclei close to the drip line range from 0.1 to 1 MeV, compared to the 6–8 MeV average nucleon separation energy for stable nuclei. Moreover, the weakly bound outer neutron(s) can also give rise to a large spatial extension in the nuclear matter distribution: the so-called halo structure [1,2]. These features are expected to strongly affect the reaction mechanisms in collisions induced by such nuclei, in particular at energies near the Coulomb barrier where the interplay between the various open reaction channels should be relevant. Particularly, one might expect that direct processes such as transfer and breakup are enhanced. Selected transfer channels may, in fact, be favored by large positive Q values or by the halo structure of the exotic nucleus. On the other hand, the low breakup threshold associated with the low binding energy of the valence neutron(s) implies that the halo projectile, approaching the Coulomb or nuclear field of a stable target nucleus, can easily break up into core and valence nucleons. Consequently, the breakup channel is expected to have a larger cross section compared with stable well-bound nuclei.

A question that is still not clear concerns the halo structure effects on the fusion cross section. A great effort has been devoted to study fusion reactions at energy near and below the Coulomb barrier when using halo nuclei as projectiles and complete reviews on this topic can be found in [3,4]. In low-energy collisions induced by halo projectiles, one can expect that the diffuse halo structure (i.e., a larger radius) implies a reduction in the fusion barrier height and therefore may lead to an enhanced fusion cross section around and below the barrier. These are known as static effects in the reaction dynamics. In addition, it is well known from early studies on fusion with stable nuclei (see, e.g., [5–9]) that dynamic effects due to the coupling of the relative motion of projectile and target to their inelastic excitations or to selected transfer channels increase the sub-barrier fusion cross section. Therefore, since in halo nuclei the ground state lies close to the continuum, the coupling not only to bound but also to unbound states could be very strong and has to be considered in order to properly describe the reaction dynamics. Theoretically, this has been done by developing continuum discretized coupled channel (CDCC) calculations [4,10–12]. Although such calculations [11,12] indicate a suppression of the total fusion (TF) cross section at energies above the barrier and an enhancement below it, the energy at which the change between these behaviors is predicted and the amount of sub-barrier enhancement depend upon the adopted approximations and the phase space in the continuum considered.

From the experimental point of view the measurement of sub-barrier fusion cross sections, using radioactive beams, is quite challenging due to the very low intensities of the available

*Present address: Tractebel Engineering, Avenue Ariane 7, B-1200 Brussels, Belgium.
†Present address: University of Vigo, E-36310 Vigo, Spain.

halo beams coupled with the small cross sections involved. The experimental investigation of fusion reactions induced by light halo projectiles have been mainly performed with the two-neutron-halo ^{6}He on heavy [13–17] and medium mass targets [18,19]. This is because ^{6}He beams are available in several radioactive beam facilities with good intensities (up to 10^7 pps). The common feature observed in most of the reactions involving the two-neutron-halo ^{6}He is the important direct process contribution, in particular transfer. However, from an analysis of the available data, controversial conclusions concerning the presence of a possible enhancement on the sub-barrier fusion cross section have been reached by different authors, either because most of the data stop at energies at which the enhancement would be readily apparent or because of the large errors, especially in the sub-barrier fusion data. Moreover, all these conclusions have been reached by performing different types of analysis and in most of the published papers the role played by the static and dynamic effects in the observed final result is not always clearly discriminated [13–20].

In conclusion, in order to solve the controversy about the presence of suppression or enhancement effects in the fusion cross section and to disentangle static and dynamic effects better quality data are needed.

We have extended the study of the elastic scattering, fusion, and transfer + breakup channels for the reaction ^{6}He + ^{64}Zn, which we had already measured at energies around the barrier [18,21], up to energies above the Coulomb barrier, V_{CB} (about twice as much). In order to point out the influence of the ^{6}He halo structure on the reaction mechanisms, the data were compared with the ones of the reaction ^{4}He + ^{64}Zn measured in the same experiment. The fusion cross section was measured by using an activation technique (see Sec. IV for details), already successfully applied as widely discussed in [18]. Preliminary results on fusion have been published in [22]. In this paper we will discuss the results for the fusion and transfer + breakup processes for the two reactions whereas the elastic scattering data obtained from this experiment will be published elsewhere.

Moreover, since our ^{4}He data explored a smaller energy range than the ^{6}He ones, we have recently performed a new experiment, using the same technique, in order to extend the fusion excitation function for the ^{4}He + ^{64}Zn system to lower energies and compare the two excitation functions up to the lowest energy data point measured for the ^{6}He-induced reaction in [18].

II. THE EXPERIMENTAL SETUP

The experiment on the ^{4,6}He + ^{64}Zn systems at energies above the barrier was performed at the Centre de Recherches du Cyclotron at Louvain la Neuve (Belgium). A radioactive beam of ^{6}He at $E_{\rm lab} = 15$ and 18 MeV with an average current of 10^6 pps, together with a stable beam of ^{4}He at $E_{\rm lab} =$ 17.5 MeV, were used. In particular the ^{4}He incident beam energy was chosen in order to measure the fusion excitation function and the elastic scattering angular distributions for the two systems, ^{4,6}He + ^{64}Zn, in the same center-of-mass energy range. The experimental setup is sketched in Fig. 1. Three arrays of silicon strip detectors surrounding a thin ^{64}Zn target were used to detect the light charged particles produced in the reaction. The target used to measure the elastic scattering and light charged particle angular distributions was a 530 μg/cm^2 self-supporting ^{64}Zn foil. It was tilted by 45° with respect to the beam direction in order to measure at laboratory angles around 90°. The detectors used were seven sectors of LEDA-type silicon strip detectors [23] and two double-sided silicon strip detectors (DsSSDs). The first array, named LEDA in Fig. 1, consists of four LEDA sectors, 300 μm thick, placed in an annular configuration with each sector normal to the beam direction at a distance of about 60 cm from the target, covering the laboratory angular range $5° \leqslant \theta \leqslant 12°$. Such a configuration allows us to monitor the beam misalignment with respect to the target. The other three LEDA sectors, 500 μm thick, were placed at 45° with respect to the beam axis, at a distance of 130 mm, covering the angular range $22° \leqslant \theta \leqslant 65°$ and allowing for a very large solid angle coverage. This configuration of the LEDA sectors is called LAMP due to its lampshade shape. The two DsSSDs were placed around 90° and covered the angular range $67° \leqslant \theta \leqslant 120°$. The distance between the detector active area and the target was about 85 mm for both DsSSDs. This detector geometry allowed for a very large angular coverage with good granularity. The fusion cross section was measured by using an activation technique irradiating a stack of ^{64}Zn targets separated by Nb catchers, as will be discussed in detail in Sec. III.

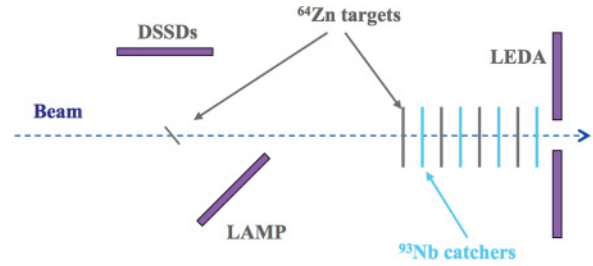

FIG. 1. (Color online) Schematic view of the experimental setup.

A total of three runs were performed with the ^{6}He beam. In the first run we measured the reaction ^{6}He + ^{64}Zn at $E_{\rm lab} =$ 15 MeV and only light charged particles were detected. The other two runs (one short and one long) were performed at 18 MeV for the activation measurements (see Sec. IV A for details). In these two runs, while irradiating the target stack, we also measured at the same time with the thin target the elastic scattering and other reaction channels.

III. DIRECT CHANNELS: TRANSFER AND BREAKUP

As discussed in Sec. I, breakup and transfer channels and their effects are expected to be important for light halo nuclei and indeed most of the reactions involving the two-neutron-halo ^{6}He nucleus (i.e., ^{6}He + ^{209}Bi [24,26–28], ^{6}He + ^{238}U [15], ^{6}He + ^{64}Zn [18], ^{6}He + ^{63,65}Cu [19,29], ^{6}He + Pb [16], and ^{6}He + ^{197}Au [17]) have shown a large near- and sub-barrier direct reaction cross section dominating the total reaction cross

section and in some cases larger than the fusion cross section by orders of magnitude.

In the present experiment, the transfer and breakup events were also analyzed, at all the energies studied, by looking at the α particle emitted in the ^{6}He + ^{64}Zn reaction. Helium isotopes were discriminated from hydrogen by the time of flight (TOF) technique using the cyclotron RF as time reference. The energy spectrum corresponding to He isotopes for the reaction ^{6}He + ^{64}Zn at $E_{\rm lab} = 18$ MeV, obtained by selecting the helium locus in the ToF-energy spectrum at $\theta = 63^{\circ}$, is shown in Fig. 2(a). In Fig. 2(b) is shown, for comparison, the He energy spectrum for the reaction ^{4}He + ^{64}Zn at the same center-of-mass energy and at the same angle. As one can see in Fig. 2(a), besides the ^{6}He elastic scattering peak and the inelastic scattering peak, corresponding to the first excited state of the target ^{64}Zn (2+), a broad bump corresponding to a large yield of α particles is present. In contrast, such events are not observed with the ^{4}He beam, as can be seen in Fig. 2(b). In the ^{6}He + ^{64}Zn collision, α particles are expected to be produced in fusion evaporation, one- and two-neutron

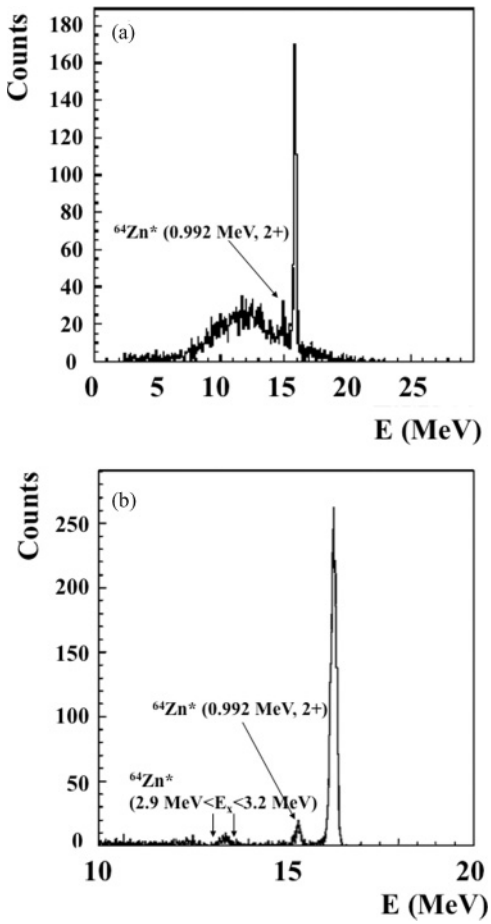

FIG. 2. (a) Energy spectrum of α and ^{6}He locus measured at $\theta = 63^{\circ}$ for the collision ^{6}He + ^{64}Zn at 18 MeV. (b) Energy spectrum for the collision ^{4}He + ^{64}Zn at $\theta = 63^{\circ}$ and at the same center-of-mass energy. In the latter, besides the inelastic scattering of the first excited state of the target ^{64}Zn ($E_x = 0.992$ MeV, 2+), a peak corresponding to the inelastic excitation contribution of a series of ^{64}Zn excited levels in the excitation energy range between 2.9 and 3.2 MeV is present.

transfer, and breakup processes. Our aim is to investigate which mechanism is responsible for such a strong production of α particles. As widely discussed in [18,21], in our case it is not easy to discriminate between transfer and breakup channels on the basis of the energies of the α particle only, since the two processes will produce events in approximately the same α energy region. According to the semiclassical condition of trajectory matching [30], the contribution due to one- ($Q_{g.g.} = 6.11$ MeV) or two-neutron ($Q_{g.g.} = 18.06$ MeV) transfer to the ground state is expected to be negligible since the optimum Q value for neutron(s) transfer is ~0. Therefore the broad peak in Fig. 2(a) represents the α-particle energy distribution where both $1n$ and $2n$ transfer as well as breakup channels are contributing. The different mechanisms cannot be disentangled but they can be discriminated from fusion on the basis of their angular distributions. Figure 3 shows the α-particle angular distributions for ^{6}He + ^{64}Zn at $E_{\rm lab} = 13$, 15, and 18 MeV. They were obtained by subtracting the elastic and the inelastic scattering contributions with a three-Gaussian fit corresponding to the ^{6}He elastic and inelastic scattering peak and the α-particle broad bump. The most forward angles were excluded since the elastic scattering contribution at those angles was too strong to be subtracted. In the same figures are also shown the angular distributions for the α particles produced in the fusion-evaporation reaction calculated by using the Monte Carlo PACE4 [31] code at the same energies. They have been arbitrarily normalized at the largest measured angle, as will be explained in Sec. IV. Since the heavy compound nucleus is produced with a very small velocity and a low angular momentum ($J_{\rm max} \sim 10\hbar$ for $E_{\rm lab}(^{6}{\rm He}) = 18$ MeV as predicted by CASCADE [32]), the α particles emitted in fusion-evaporation processes are expected to have an almost isotropic angular distribution, as can be seen from Fig. 3. On the other hand, the angular distribution of α particles produced in direct reactions, such as for instance transfer and breakup, is expected to be peaked around the grazing angle with a maximum that moves at forward angles as the beam energy increases. Therefore, from the behavior of the measured α-particle angular distributions and from the comparison with the calculated ones it is evident that most of the detected α particles are coming from direct processes.

The transfer + breakup integrated cross section, obtained by assuming $d\sigma/d\theta = 0$ at $\theta_{\rm lab} = 0^{\circ}$ and 180° at 15 MeV and 150° at 18 MeV, are $\sigma = (895 \pm 90)$ mb and $\sigma = (1088 \pm 76)$ mb at $E_{\rm lab} = 15$ and 18 MeV, respectively. The transfer + breakup cross section at $E_{\rm lab} = 13$ MeV has been extracted in [18] and is $\sigma = (1200 \pm 150)$ mb. From the comparison of the transfer + breakup cross sections with the total reaction (TR) cross section, extracted from an optical model analysis performed on the ^{6}He + ^{64}Zn elastic scattering angular distributions at the two energies studied, we have observed that the largest fraction of the TR cross section, about 70%, corresponds to transfer and breakup channels. This result is consistent with the large α-particle cross section arising from direct processes measured for the reaction ^{6}He + ^{64}Zn at energies around the barrier in our previous experiment [18,21]. Moreover, as discussed in [21], evidence that some of the α particles are produced in transfer processes clearly emerges from the data analysis. An analysis of events where two

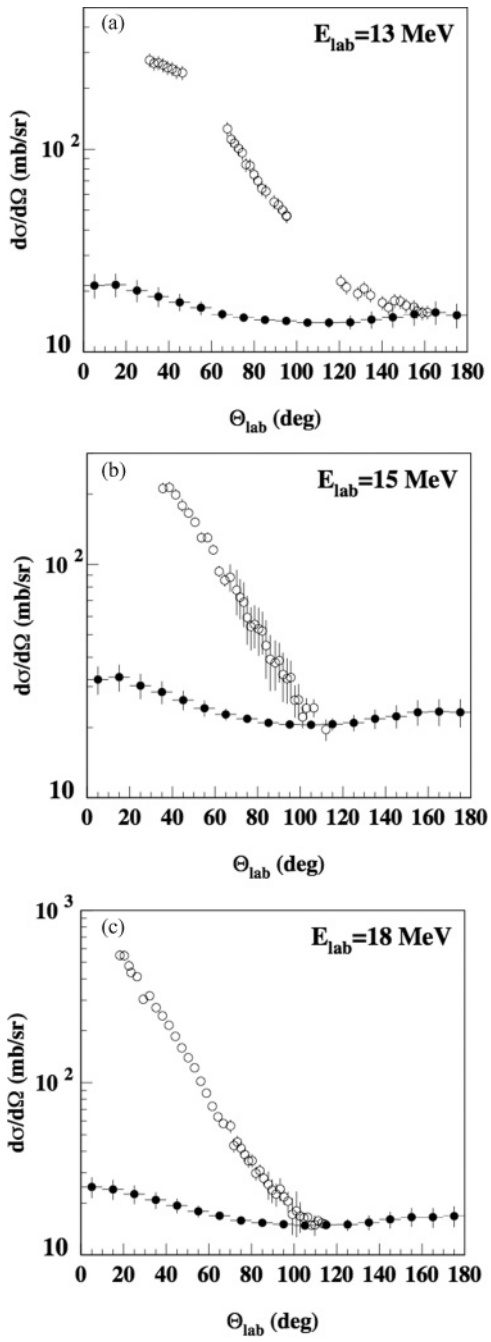

FIG. 3. Top (a), middle (b), and bottom (c) α-particle angular distributions for ^{6}He + ^{64}Zn at $E_{\rm lab}$ = 13, 15 and 18 MeV, respectively (open circles). The closed circles represent the α-particle angular distributions calculated by using the PACE4 code and normalized at the largest measured angle. See text for details.

charged particles were detected in coincidence showed that two-neutron transfer events were certainly present [21]. As shortly discussed in Sec. I, some recent works [28,29] have also pointed out that the 2*n* transfer plays a major role in the low-energy collisions induced by the ^{6}He nucleus. In [28] the contribution originated from breakup and from one- and two-neutron transfer processes for the system ^{6}He + ^{209}Bi has been separated using neutron-α coincidence measurements. The authors found that at energies around the barrier most of the α-particle yield, about 75%, derives from 1*n* transfer (about 20% [26]) and 2*n* transfer (about 55% [27]), and the remaining 25% from direct breakup [28]. A similar result has been observed in [29] on the ^{6}He + ^{65}Cu reaction where triple coincidence among α particles, neutrons, and γ rays in ^{66}Cu has been measured. Chatterjee *et al.* [29] found that, also for this system, the transfer cross section is very large.

Therefore, the results obtained in the present work confirm that in collisions induced by the two-neutron-halo ^{6}He nucleus, direct processes, such as transfer and breakup, have a dominant role in the reaction mechanisms and dominate the TR cross section also at energies above the barrier.

IV. FUSION CROSS SECTION

A. Activation measurements

The ^{4,6}He + ^{64}Zn fusion cross sections were measured by using an activation technique based on the off-line measurement of the x-ray emission following the electron capture (E.C.) decay of the evaporation residues (E.R.) produced in the reactions. The same technique has been already successfully applied to measure the ^{4,6}He + ^{64}Zn fusion excitation function at lower energies [18]. This technique turned out to be particularly suitable for our systems since, with the help of statistical model calculations, we have chosen the target nucleus so that the formed radioactive residues decay mainly by E.C. Indeed, statistical model calculations, performed with the CASCADE code, predict that the contribution of stable E.R. for the two studied systems is at most 10% of the total fusion cross section.

A stack of four thick ^{64}Zn targets (∼2 mg/cm^2) alternated with the same number of ^{93}Nb catcher foils (∼3 mg/cm^2) was placed about 60 cm downstream of the thin ^{64}Zn target. The role of the ^{93}Nb catchers, placed immediately behind each ^{64}Zn thick target, was twofold: to stop the residues emerging from the previous target and to reduce progressively the beam energy, thus increasing the average difference in beam energy for the different targets. In such a way, it is possible to extract the cross section at different energies without changing the beam energy, thus reducing the beam time needed to perform an excitation function measurement with the very low intensity radioactive beams. By activating these stacks, center-of-mass energy ranges of $12.7 \leqslant E_{\rm c.m.} \leqslant 16.1$ MeV in the ^{6}He-induced reactions and $13.6 \leqslant E_{\rm c.m.} \leqslant 16.2$ MeV in the ^{4}He case were explored.

The delayed x-ray target activity was detected off-line by using lead-shielded large-area ORTEC lithium-drifted silicon detectors, Si(Li), whose intrinsic efficiency is 100% for x-ray energies of interest (around 10 keV). With this technique, it was possible to measure counting rates as low as 0.5 counts/h for about 1 month, collecting enough statistics even for the E.R. with the lowest cross section of about 3 mb. The x-ray activity emitted by each ^{64}Zn foil was measured by placing both the ^{64}Zn target and the ^{93}Nb catcher very close (∼10 mm) to the Si(Li) detector. The ^{93}Nb foil was placed on top of the ^{64}Zn foil so that they were measured simultaneously. Possible reactions induced by the beam on the ^{93}Nb catchers do not represent a

problem since the x-ray energies are different from the ones corresponding to reactions on ^{64}Zn. Each measurement was repeated several times for each target for a period of about one year in order to measure the activity as a function of time.

In the present experiment, a short irradiation run (irradiation time $t_i \sim 7$ hr) was performed with the stable ^{4}He beam with an average beam current of 10^8 pps. In order to optimize the production of E.R. with different half-lives, one short activation run and one long activation run, $t_i \sim 6$ hr and $t_i \sim 3$ days, respectively, were performed with the radioactive ^{6}He beam with an average current of 10^6 pps. In order to detect the activity of the short-lived residues (^{67}Ge, ^{68}Ga, ^{67}Ga, and ^{64}Cu), the irradiated targets were measured off-line shortly after the end of the activation at the LLN facility. To detect very long lived activity (^{68}Ge and ^{65}Zn), the decay spectra, for the foils irradiated during the ^{6}He long activation run, were collected at the Laboratori Nazionali del Sud in Catania for a period of about one year after the end of the irradiation. The incident beam current during the irradiation has been measured with Rutherford scattering on the thin primary ^{64}Zn target.

As mentioned in Sec. I, we have extended the measurement of the fusion excitation function for the ^{4}He + ^{64}Zn system at lower energies, using the same activation technique. In this case, the activation experiment was performed at the Tandem Accelerator of the Ruder Bošković Institute (RBI) in Zagreb with an average ^{4}He beam current of 5×10^{10} pps. Five short ($t_i \sim 30$ min) irradiation runs were performed. We have irradiated five ^{64}Zn foils, each one backed by a ^{93}Nb catcher, one at a time, at five beam energies ranging from 8.1 to 10.6 MeV. The beam energies were chosen in order to achieve the overlap with the previous ^{4}He + ^{64}Zn data [18] and to measure the fusion cross section for the ^{4}He + ^{64}Zn system down to the lowest energy data point measured for the ^{6}He-induced reaction [18]. The incident beam current was measured with a Faraday cup with an accuracy of about 5%.

B. Analysis of the x-ray spectra

As explained in [18], the E.R. were identified in charge from their characteristic x-ray energies, whereas different isotopes were disentangled by their decay half-lives. In Tables I and II the identified heavy reaction products along with their fusion-evaporation decay chain and their half-lives, for the reactions ^{4,6}He + ^{64}Zn, respectively, are listed.

Typical x-ray spectra for the ^{6}He + ^{64}Zn reaction are shown in Figs. 4(a) and 4(b). For each element, two peaks are present, corresponding to the Kα and Kβ x-ray emission. The Kβ emission represents about 15% of the total x-ray emission, and thus the analysis was performed only on the Kα lines. Figure 4(a) shows the x-ray spectrum corresponding

TABLE I. Identified evaporation residues for the ^{4}He + ^{64}Zn reaction.

E.R.	Decay chain	$T_{1/2}$
^{67}Ge	1n	18.9 min
^{67}Ga	1p	3.26 d

TABLE II. Identified evaporation residues for the ^{6}He + ^{64}Zn reaction.

E.R.	Decay chain	$T_{1/2}$
^{68}Ge	2n	270.82 d
^{68}Ga	1n-1p	67.6 min
^{67}Ge	3n	18.9 min
^{67}Ga	2n-1p	3.26 d
^{65}Zn	1n-α	244.26 d
^{64}Cu	1n-1p-α	12.7 hr

to the target activated at the highest energy, $E_{\text{c.m.}} = 16.4$ MeV, measured about 3 min after the irradiation run ended. From the x-ray energies one can clearly identify the Kα contribution due to the decay of Ge, Ga, Zn, and Cu isotopes. The spectrum is dominated by the decay of the short-lived Ga isotopes although the lines from the long-lived Zn and Ge isotopes are also visible. In Fig. 4(b) a spectrum relative to the same target, but collected over one week, starting about one month after the end of the activation is shown. The peak corresponding to Ga isotopes is strongly reduced, since the half-life of the longest lived Ga isotope produced in the reaction is 3.26 d. In

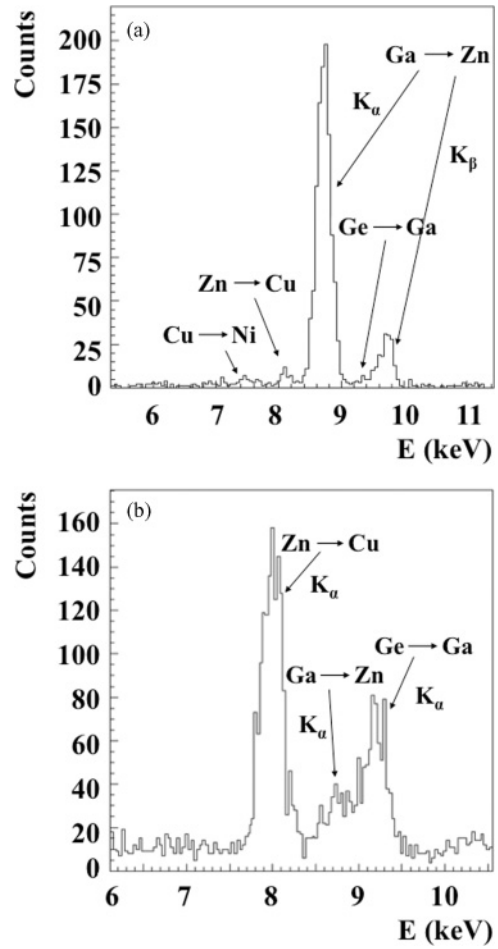

FIG. 4. The x-ray spectra, for the target activity with the ^{6}He beam at $E_{\text{c.m.}} = 16.4$ MeV, obtained shortly after the end of the activation (a) and about one month after the end of the activation (b).

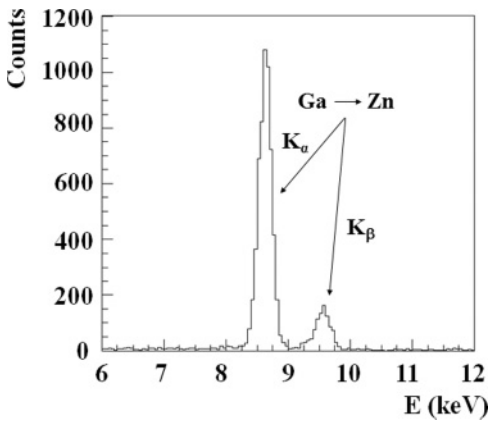

FIG. 5. The x-ray spectra obtained in the ^{4}He irradiation run at $E_{\rm lab} = 10.4$ MeV.

contrast, in this spectrum, owing to the long collection time, the contribution of long-lived Zn and Ge isotopes becomes dominant. As one can see, the background level, not subtracted in this figure, is very small. The background underneath the peak of interest has been evaluated by integrating a region in the spectrum where there were no evident peaks. In such a way, the average background contribution per channel was extracted and then multiplied for the number of channels where the peak of interest contributes.

In Fig. 5 is shown a x-ray spectrum for the ^{4}He irradiation at $E_{\rm lab} = 10.4$ MeV recently performed at the RBI Tandem Accelerator Facility in Zagreb. As one can clearly see from the x-ray energies, only the contribution due to the decay of Ga isotopes is present. Actually, according to the statistical model predictions, in the ^{4}He + ^{64}Zn reaction two radioactive E.R. are produced, i.e., ^{67}Ge and ^{67}Ga. ^{67}Ge is a short-lived nucleus, with a half-life of 18.9 min; thus it is very difficult to follow the activity as a function of time for each target with the technique we used. However, ^{67}Ge decays by E.C. 100% into ^{67}Ga and therefore the total fusion cross section was extracted from the ^{67}Ga x-ray lines alone.

As previously mentioned, the contribution due to the different elements can be disentangled from the x-ray energies. Although different isotopes of the same species cannot be identified by the x-ray energies, they have been discriminated by following the activity as a function of time and by fitting it using the known half-lives. Plotting these data on a semilogarithm graph [that is, ln(activity) versus time] should give a straight line of slope of $-\lambda$, the decay constant. This method is particularly suitable in the present case since the half-lives of the E.R. are neither too short nor too long. The produced residues have half-lives ranging between one hour to almost one year, as shown in Tables I and II for ^{4}He + ^{64}Zn and ^{6}He + ^{64}Zn, respectively. Figures 6(a) and 6(b) show the activity curve for the Ga isotopes extracted in the activation run with the ^{6}He beam at $E_{\rm lab} = 15$ MeV and with the ^{4}He beam at $E_{\rm beam} = 10.4$ MeV, respectively. The time $T = 0$ corresponds to the end of the irradiation. The activity curve in Fig. 6(a) shows two different slopes corresponding to the decay of two gallium isotopes, ^{67}Ga and ^{68}Ga. It was fitted by assuming the simultaneous contribution of the two gallium isotopes, in

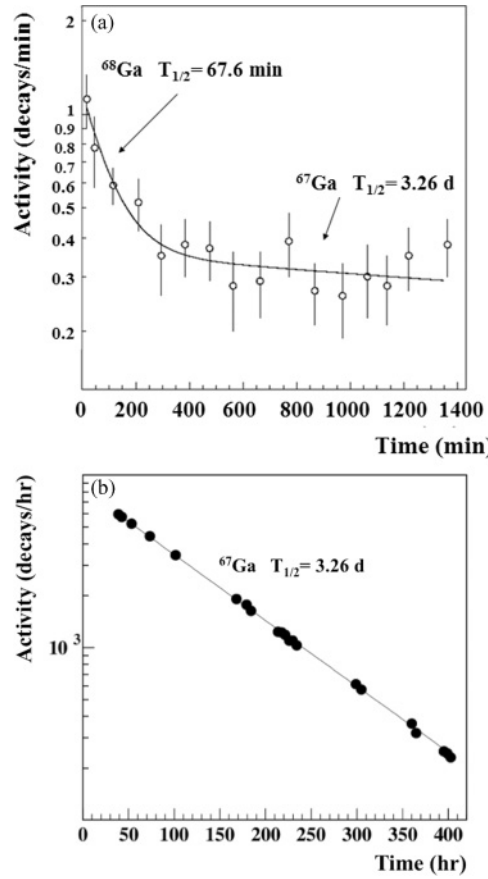

FIG. 6. (a) Activity curve for the Ga isotopes extracted in the activation run with the ^{6}He beam at $E_{\rm beam} = 15$ MeV. The contributions of ^{68}Ga and ^{67}Ga can be disentangled using their different half-lives. (b) Activity curve for the Ga isotope extracted in the activation run with the ^{4}He beam at $E_{\rm beam} = 10.5$ MeV. Only the contribution of one gallium isotope, ^{67}Ga, is present.

agreement with CASCADE predictions. In contrast, in the run with the ^{4}He beam [Fig. 6(b)] the activity curve shows only the presence of one gallium isotope, ^{67}Ga, and thus in this case the curve was fitted by assuming only the contribution of this isotope.

Following this procedure the contributions of the different radioactive heavy fragments were unfolded for each target (i.e., each activation energy).

C. Determination of cross sections

The determination of the production cross sections of the heavy fragments from the x-ray activity measurements requires knowledge of the number of incident beam particles, the thickness of the different targets (i.e., the number of target atoms), the total x-ray detection efficiency, and the Kα fluorescence probability. The fluorescence probability was taken from [33]. The beam current was determined from elastic scattering at small angles where the elastic cross section is known to be Rutherford. However, for the short-lived nuclides, in order to evaluate the number of produced radioactive nuclei that decay during the activation time, it was necessary to

measure the beam current as a function of time, during the irradiation run. Therefore, a clock signal was generated by using the signal of a pulse generator with a fixed and stable frequency. This signal was stored on disk along with the elastic scattering data. A spectrum of time versus counts in the elastic peak at small angles was extracted from the data with a 1-min time bin and, after normalization, the incident current as a function of time was obtained. The target thickness was measured by the energy loss of 5.48 MeV α particles traversing the foil. The Si(Li) geometric detection efficiency was calculated by using a Monte Carlo simulation code. The incident beam profile was measured, before starting the activation run, by replacing the stack with a CsI scintillator and in order to measure the beam spot size a grid was glued on the CsI. The beam profile, which was elliptical in shape, was reproduced by using a Gaussian distribution along both the x and the y axes. Thus, the beam profile along with the detector geometry was folded into the Monte Carlo code. Finally, knowing, from the analysis of the activity curves, the experimental activity at $T = 0$ for each isotope it was possible to extract the production cross sections for all radioactive heavy fragments produced in the target.

The excitation functions were obtained by summing, at each activation energy, the contribution of all radioactive heavy fragments produced in the two reactions ^{4,6}He + ^{64}Zn. Actually, the heavy fragment cross section for the ^{4}He + ^{64}Zn system coincides with the fusion one since for this reaction fusion is the only process which contributes to the production of the heavy fragments. Figure 7 shows a comparison between the heavy-fragment excitation function for the ^{4}He + ^{64}Zn reaction (squares) and for the ^{6}He + ^{64}Zn reaction (diamonds). The data in the energy range $7 \leqslant E_{\mathrm{c.m.}} \leqslant 12$ MeV shown in Fig. 7 are those we previously measured with the same technique [18].

The uncertainties on the cross section reflect the statistical and the systematic errors arising from the integration of the beam current, the detection efficiency, the decay branching ratios, and the target thickness. The uncertainty on the experimental activity is the statistical error on the Kα peak

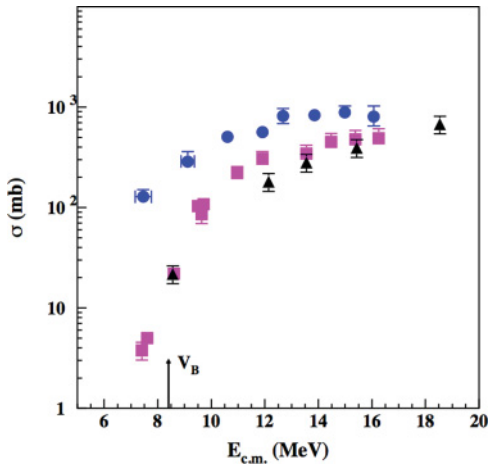

FIG. 7. (Color online) Heavy-fragment excitation functions for the ^{4}He + ^{64}Zn reaction (squares) and for the ^{6}He + ^{64}Zn reaction (circles). The triangles represent the ^{4}He + ^{64}Zn data taken from [35].

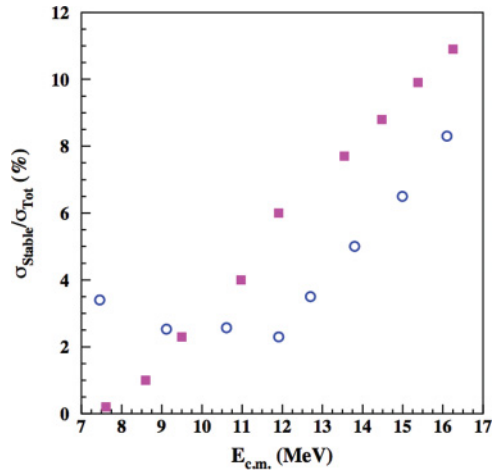

FIG. 8. (Color online) Fraction of the stable E.R. with respect to the fusion cross section, calculated with the CASCADE code, as a function of the center-of-mass energy for the ^{4}He + ^{64}Zn reaction (squares) and for the ^{6}He + ^{64}Zn reaction (circles).

integral. The uncertainty on the decay constant and on the fluorescence probability are the values listed in [33]. The uncertainty on the simulation of the detection efficiency depends on the determination of the distance between the Zn foil and the Si(Li) detector surface. The latter is affected by an error of about 1 mm and produces an uncertainty on the total detection efficiency of about 10%. The uncertainty on the beam current corresponds to the systematic error on the normalization of the Rutherford scattering cross section and is about 5%. The error in the target number per square centimeter arises from the uncertainty in the target thickness, measured by the energy loss of 5.48-MeV α particles traversing the foils. The source of the error is due to the energy loss calculation and is of the order of 2%. The error bars also include the contribution of the stable E.R., estimated with the help of the CASCADE code, not measured in the experiment. The statistical model predictions for the fraction of the stable E.R. with respect to the fusion cross section, shown in Fig. 8, are between 2.3 and 8.3% for the ^{6}He + ^{64}Zn reaction and between the 0.2 and 11% for the ^{4}He + ^{64}Zn reaction.

The energy error bars in the ^{6}He + ^{64}Zn data points, taken from [18], represent the energy spread of the ^{6}He beam in the Zn and Nb rolled foils. This energy spread includes not only the contribution of the energy straggling calculated also in [18] (due to the statistical nature of the collisions between the beam ions and the target atoms) but also the contribution due to the nonuniformity of the foil thickness. Indeed, the energy straggling due to the nonuniformity of the foil thickness has been shown to be relevant, in particular when using rolled foils, [34]. All the details about the procedure we have adopted to estimate this effect on the energy spread will be discussed in a following paper.

The ^{4}He + ^{64}Zn data between 7 and 10 MeV in Fig. 7 represent the results of the new measurements performed at the Tandem Accelerator Facility in Zagreb (see Sec. IV). One can notice the very good overlap achieved at $E_{\mathrm{c.m.}} = 9.8$ MeV between the ^{4}He + ^{64}Zn data set published in [18] and the more recently ones presented in this work. In Fig. 7 are also

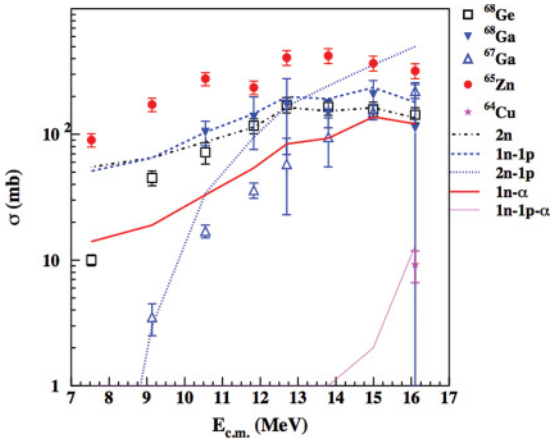

FIG. 9. (Color online) Experimental radioactive heavy-fragment cross sections as a function of the center-of-mass energy for the ^{6}He + ^{64}Zn reaction. The lines correspond to the statistical model predictions, obtained with the code CASCADE, for the E.R. formed in the decay of ^{70}Ge.

shown the ^{4}He + ^{64}Zn data measured by Ruddy and Pate in the late 1960s by using a radiochemical method [35]. One can see the overall agreement of the ^{4}He + ^{64}Zn fusion cross sections extracted in this work with the ones of [35]. Comparing the ^{4,6}He + ^{64}Zn excitation functions of Fig. 7, we observe a strong enhancement of the heavy-fragment cross sections in the reaction induced by the halo ^{6}He beam, in particular at sub-barrier energies. Such enhancement in the production cross section of the heavy fragments was already observed in [18] and was mainly attributed to the contribution of a single residue (^{65}Zn).

Figure 9 shows a comparison between the experimental cross sections (symbols) for each fragment produced in the ^{6}He + ^{64}Zn reaction as a function of the center-of-mass energy and the results of statistical model calculations, performed with the CASCADE code, for the E.R. formed in the decay of the compound nucleus, ^{70}Ge. As one can see, the measured cross section for ^{65}Zn, i.e., the α-n evaporation channel, far exceeds, in all energy ranges explored, the statistical model prediction. A possible explanation for this large discrepancy is that other mechanisms are contributing to this particular channel. Actually, as discussed in [18], ^{65}Zn is formed in the α-n fusion evaporation process but one- and two-neutron transfer leads to the formation of this nucleus as well. Indeed, an indication of a strong transfer component has been already observed in [21] where the transfer processes, in particular the 2n transfer reactions, have been identified by looking at backward-angle α-α and α-p coincidence events.

In order to estimate an upper limit for the cross section of the α fusion-evaporation channel we have looked at the angular distributions of the α particles emitted in the ^{6}He + ^{64}Zn reaction (see Sec. III). As discussed in Sec. III, from the behavior of the measured α-particle angular distributions, shown in Fig. 3, the origin of such α particles has been attributed to direct processes. In Fig. 3 are also shown the angular distributions of the α particles emitted from fusion-evaporation, calculated with the Monte Carlo PACE4 code, arbitrarily normalized to the experimental ones at the largest measured angle. From the comparisons in Fig. 3 it is clear that the shape of the measured α-particle angular distributions, in particular at $E_{\rm lab}$ = 15 and 18 MeV, is steep even at the most backward angles and completely different from the one expected for α particles coming from fusion-evaporation, as calculated with PACE4. Thus, one can conclude that even at the largest measured angle the contribution due to direct processes is important and that in this angular region the fusion-evaporation process is not the only one contributing to the production of the α particles. Therefore, the cross sections extracted by integrating the PACE4 angular distributions arbitrarily normalized to the most backward angles represent an upper limit for the cross sections of the α particles emitted in fusion-evaporation channels, since to extract them we have assumed that fusion-evaporation is the dominant process at the largest measured angle. The integrated cross sections corresponding to an upper limit for the evaporated α particles are (195 ± 16), (282 ± 25), and (211 ± 13) mb at $E_{\rm lab}$ = 13, 15 and 18 MeV, respectively.

Consequently, the extracted cross sections represent also an upper limit for the α-n fusion-evaporation process contribution to the production of ^{65}Zn. Figure 10 shows the upper limit for the evaporated α-particle cross sections at the three energies $E_{\rm lab}$ = 13, 15, and 18 MeV along with the ^{65}Zn experimental cross sections, the ^{65}Zn CASCADE predictions, and the α evaporation channel CASCADE predictions. As can be seen in Fig. 10 the ^{65}Zn cross section is even larger than the extracted upper limit and the experimental overabundance must be attributed to a large contribution coming from one- and two-neutron transfer reactions.

A similar analysis has been also performed for the hydrogen isotopes for the ^{6}He + ^{64}Zn data of [18,21]. In Fig. 11 are shown the comparisons between the measured angular distributions for protons emitted in the ^{6}He + ^{64}Zn reaction at $E_{\rm lab}$ = 10 and 13 MeV and the ones for protons produced in the fusion-evaporation process, calculated with PACE4 and arbitrarily normalized to the experimental ones. As one can

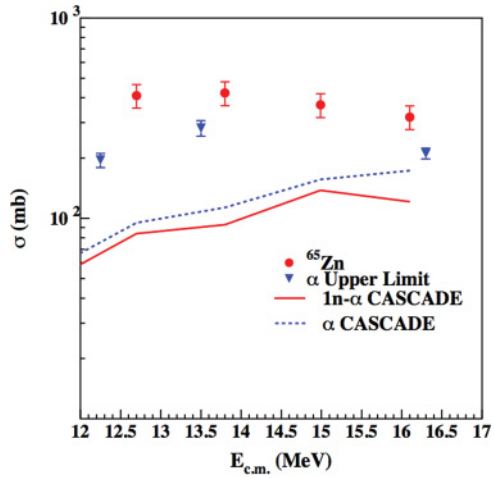

FIG. 10. (Color online) Measured cross sections (circles) as a function of the center-of-mass energy and statistical model predictions (solid line) for the ^{65}Zn residue and for the α fusion-evaporation channel (dashed-line). The triangles represent the upper limit for the α-n fusion-evaporation process contribution to the production of ^{65}Zn at the three energies $E_{\rm lab}$ = 13, 15, and 18 MeV.

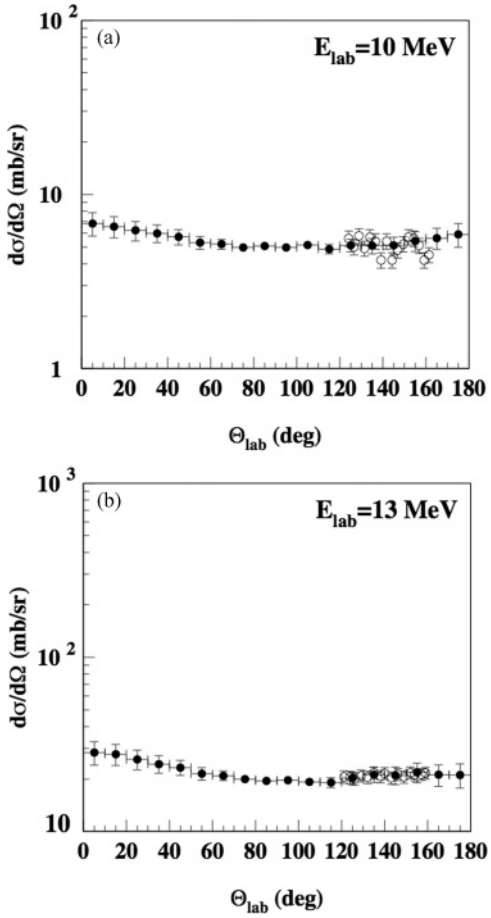

FIG. 11. Top (a) and bottom (b) proton angular distributions for ^{6}He + ^{64}Zn at $E_{\rm lab}$ = 10 and 13 MeV, respectively (open circles). The closed circles represent the proton angular distributions calculated by using the PACE4 code. See text for details.

see, contrary to what is observed for the α-particle angular distributions, the behavior of the proton angular distributions, in the measured angular range, is well reproduced by the one calculated with PACE4, indicating that the protons are mostly produced in fusion-evaporation rather than direct processes. Moreover, the cross section extracted by integrating the PACE4 proton angular distribution arbitrarily normalized to the experimental one at $E_{\rm lab} = 13$ MeV, $\sigma = (265 \pm 21)$ mb, is well in agreement with the experimental cross section measured for ^{68}Ga plus ^{67}Ga fragments [$\sigma = (231 \pm 110)$ mb], i.e., the p evaporation channels. At $E_{\rm lab} = 10$ MeV the extracted cross section for protons, $\sigma = (66 \pm 7)$ mb, is compared with the CASCADE prediction for ^{68}Ga ($\sim$65 mb), the $1n$-$1p$ evaporation channel, and the measured cross section for ^{67}Ga [$\sigma = (4 \pm 1)$ mb] and a good agreement is achieved at this energy as well.

D. Fusion excitation function

In order to subtract the contribution due to transfer in the ^{65}Zn data, as already done in [18], the measured value for ^{65}Zn was replaced with the one calculated using the CASCADE code. The ^{4,6}He + ^{64}Zn fusion excitation functions, obtained with the above-described technique are shown in Fig. 12. From the comparison, the fusion excitation functions for the two systems appear to be rather similar at energies above the Coulomb barrier but a sub-barrier enhancement of the fusion cross section is present in the case of ^{6}He with respect to the ^{4}He one. From these results it is clear that the strong enhancement of the cross section observed in Fig. 7 for the halo nucleus case can be mainly attributed to transfer rather than to fusion. This result is in agreement with the strong transfer contribution measured by different authors in reactions induced by the ^{6}He halo nucleus [15,18,19,26,28,29]. However, once the transfer contribution is subtracted we can still observe an enhancement of the fusion cross section below the barrier. An enhancement of the fusion cross section induced by ^{6}He with respect to the one induced by ^{4}He around the barrier has been also observed in other systems, such as for instance ^{6}He + ^{209}Bi (see, e.g., [20]) and ^{6}He + ^{197}Au (see, e.g., [17]).

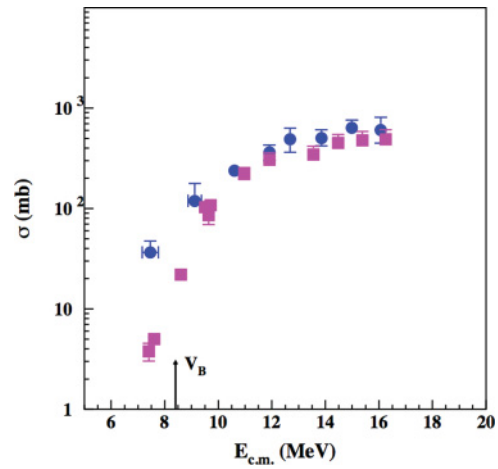

FIG. 12. (Color online) ^{4}He + ^{64}Zn (squares) and ^{6}He + ^{64}Zn (circles) fusion excitation functions. See text for details.

As discussed in Sec. I, from a survey of the existing data in the literature about the role of the halo structure in ^{6}He-induced fusion the conclusions of different authors still show controversy about possible enhancement or suppression effects, depending on how the data are compared to extract the searched effect. Indeed as suggested in [36], in order to disentangle static and dynamic effects, when the fusion excitation functions for halo nuclei are compared with those induced by well-bound nuclei on the same target nucleus, it is necessary to remove the static effects due to the large radial extent of the halo matter density distribution. In such a way the possible enhancement or suppression effect on the fusion cross section can be attributed to the coupling to the different channels, only.

A possible way to consider the static effects consists in taking into account the dependence of the system size and the Coulomb barrier height on the mass and the charge of the nuclei as suggested in [37]. Thus, we have divided the cross section by $(A_P^{1/3} + A_T^{1/3})^2$ and the center-of-mass energy by $(Z_P Z_T)/(A_P^{1/3} + A_T^{1/3})$, where A_P and Z_P and A_T and Z_T are masses and charges of the projectile and target, respectively. The results are presented in Fig. 13, where

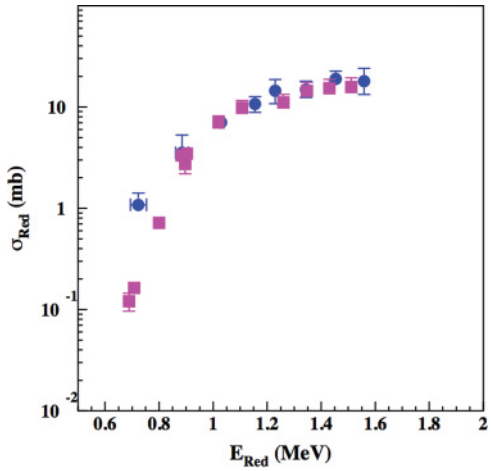

FIG. 13. (Color online) ^{4}He + ^{64}Zn (squares) and ^{6}He + ^{64}Zn (circles) fusion excitation functions normalized with respect to the geometrical factor and the height of the Coulomb barrier as suggested in [37]. See text for details.

$\sigma_{\rm Red} = \sigma/(A_P^{1/3} + A_T^{1/3})^2$ and $E_{\rm Red} = E/(Z_P Z_T)/(A_P^{1/3} + A_T^{1/3})$. As one can see at sub-barrier energies an enhancement is still observed on the fusion cross section of the ^{6}He nucleus whereas at energies above the barrier the fusion excitation functions for the two systems appear to be very similar. We remark, however, that in such a way the effect of the diffuse halo structure of ^{6}He is not explicitly considered since we are assuming that the barrier parameters depend on the atomic and mass numbers, uniquely.

If we are interested in eliminating the structure effect, due to the long tail of the halo nucleon density distribution, we should consider the dependence of the barrier radius, R_B, and the Coulomb barrier, V_B, on the nuclear structure features, as pointed out in [36], by adopting R_B and V_B values more realistic than the ones obtained from the systematic. Figure 14 shows our data, reduced by normalizing the cross section with respect to the quantity πR_B^2 and by subtracting the energy for the height of the Coulomb barrier V_B. The R_B and V_B values

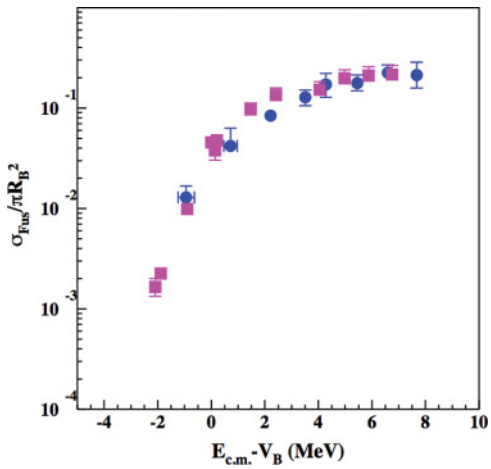

FIG. 14. (Color online) ^{4}He + ^{64}Zn (squares) and ^{6}He + ^{64}Zn (circles) fusion excitation functions reduced as $\sigma/\pi R_B^2$ vs $E_{\rm c.m.} - V_B$.

we used are taken from Ref. [36] and are extracted using the double-folding Sao Paulo potential [38,39] with realistic nuclear densities.

As one can see, the sub-barrier fusion enhancement is no longer present and the fusion excitation functions for the two systems appear very similar at all the measured energies. Thus, the enhancement of the fusion cross section, observed in Fig. 12, at energies below the barrier seems to be due to the structure of the halo ^{6}He nucleus rather than the coupling with other channels, as a direct consequence of the larger radius and the lower barrier of the potential for the ^{6}He + ^{64}Zn system. In [36] it has been shown that the enhancement of the fusion cross section observed for the ^{6}He + ^{209}Bi system at sub-barrier energies can be attributed uniquely to static effects, as in the present case.

V. SUMMARY AND CONCLUSIONS

This work presents a study of the collision induced by the two-neutron-halo nucleus ^{6}He on a medium-mass ^{64}Zn target at energies above and around the Coulomb barrier aiming to investigate structure effects on reaction mechanisms. The study of the elastic scattering, fusion, and transfer + breakup channels for the ^{6}He + ^{64}Zn reaction, already measured at energies around the barrier by Di Pietro *et al.* [18,21], was extended up to energies above the Coulomb barrier (about two times V_{CB}). For comparison, the reaction induced by the stable isotope ^{4}He on the same target was also measured. In this paper, results on fusion and transfer + breakup channels have been presented. To overcome the experimental difficulties of measuring low-energy fusion cross sections induced by low-intensity beams, an activation technique, detecting off-line the atomic x-ray emission following the E.C. decay of the E.R. produced in the ^{4,6}He + ^{64}Zn reactions, has been applied. The fusion excitation functions of the two systems have been measured in the same center-of-mass energy range. Moreover, the fusion cross section measurement for the ^{4}He + ^{64}Zn system was extended to lower energies with respect the previous data [18] in order to compare the two excitation functions down to the lowest energy data point measured for the ^{6}He-induced reaction in [18]. By comparing the excitation functions for the two systems ^{4,6}He + ^{64}Zn, obtained by adding at each energy the contribution of all radioactive heavy fragments produced, a strong enhancement of the heavy-fragment production cross section shows up in the reaction induced by the halo nucleus, with respect to the stable one, in the whole energy range measured. However, it has been shown that such a strong increase is only due to the contribution of a particular residue, i.e., ^{65}Zn, and that the extra yield measured for such residue can be attributed to one- and two-neutron transfer. Therefore, once this contribution is subtracted, the conclusion is that no effect on fusion cross section at energies above the barrier was observed in the ^{6}He-induced collision with respect to the one for ^{4}He whereas an enhancement of the fusion cross section is still present below the barrier. By reducing the fusion excitation functions so that the static effects originated by the diffuse halo structure are eliminated, it was concluded that the enhancement observed in the ^{6}He fusion cross section at

sub-barrier energies seems to be due to the ^{6}He halo structure rather than coupling effects.

A large yield of α particles has been measured in the ^{6}He + ^{64}Zn reaction. From the angular distributions of these α particles their origin was attributed to direct processes such as transfer and breakup. The large corresponding integrated cross sections confirm the dominant role of direct processes, observed by different authors [15,18,19,25–29], in the reaction involving the two-neutron-halo ^{6}He nucleus at energies below and above the barrier.

ACKNOWLEDGMENTS

The authors wish to thank the Nuclear Physics group of the School of Physics and Astronomy at the University of Edinburgh for providing the LEDA detectors and the electronics used in the experiment and Professor P. R. S. Gomes and Professor G. La Rana for useful discussions. We are also truly indebted to all the staff of the CRC in LLN for the excellent beam quality and the warm hospitality.

[1] P. G. Hansen and B. Jonson, Europhys. Lett. **4**, 409 (1987).
[2] P. G. Hansen, A. S. Jensen, and B. Jonson, Annu. Rev. Nucl. Part. Sci. **45**, 591 (1995), and references therein.
[3] L. F. Canto *et al.*, Phys. Rep. **424**, 1 (2006).
[4] N. Keeley, R. Raabe, N. Alamanos, and J.-L. Sida, Prog. Part. Nucl. Phys. **59**, 579 (2007).
[5] R. G. Stokstad *et al.*, Phys. Rev. Lett. **41**, 465 (1978).
[6] R. G. Stokstad *et al.*, Phys. Rev. C **21**, 2427 (1980).
[7] M. Beckerman *et al.*, Phys. Rev. Lett. **45**, 1472 (1980).
[8] M. Beckerman *et al.*, Phys. Rev. C **23**, 1581 (1981).
[9] M. Beckerman, M. Salomaa, A. Sperduto, J. D. Molitoris, and A. DiRienzo, Phys. Rev. C **25**, 837 (1982).
[10] J. A. Tostevin, F. M. Nunes, and I. J. Thompson, Phys. Rev. C **63**, 024617 (2001).
[11] K. Hagino, A. Vitturi, C. H. Dasso, and S. M. Lenzi, Phys. Rev. C **61**, 037602 (2000).
[12] A. Diaz-Torres and I. J. Thompson, Phys. Rev. C **65**, 024606 (2002).
[13] J. J. Kolata *et al.*, Phys. Rev. Lett. **81**, 4580 (1998); J. J. Kolata *et al.*, Phys. Rev. C **57**, R6 (1998).
[14] M. Trotta *et al.*, Phys. Rev. Lett. **84**, 2342 (2000).
[15] R. Raabe *et al.*, Nature (London) **431**, 823 (2004).
[16] Yu. E. Penionzhkevich, V. I. Zagrebaev, S. M. Lukyanov, and R. Kalpakchieva, Phys. Rev. Lett. **96**, 162701 (2006).
[17] A. Lemasson *et al.*, Phys. Rev. Lett. **103**, 232701 (2009).
[18] A. Di Pietro *et al.*, Phys. Rev. C **69**, 044613 (2004).
[19] A. Navin *et al.*, Phys. Rev. C **70**, 044601 (2004).
[20] N. Alamanos, A. Pakou, V. Lapoux, J. L. Sida, and M. Trotta, Phys. Rev. C **65**, 054606 (2002).
[21] A. Di Pietro *et al.*, Europhys. Lett. **64**, 309 (2003).
[22] A. Di Pietro *et al.*, Eur. Phys. J. Spec. Top. **150**, 15 (2007).
[23] T. Davinson *et al.*, Nucl. Instrum. Methods Phys. Res. A **454**, 350 (2000).
[24] E. F. Aguilera *et al.*, Phys. Rev. Lett. **84**, 5058 (2000).
[25] E. F. Aguilera *et al.*, Phys. Rev. C **63**, 061603(R) (2001).
[26] J. P. Bychowski *et al.*, Phys. Lett. B **596**, 26 (2004).
[27] P. A. De Young *et al.*, Phys. Rev. C **71**, 051601(R) (2005).
[28] J. J. Kolata *et al.*, Phys. Rev. C **75**, 031302R (2007).
[29] A. Chatterjee *et al.*, Phys. Rev. Lett. **101**, 032701 (2008).
[30] D. M. Brink, Phys. Lett. B **40**, 1 (1972).
[31] O. B. Tarasov and D. Bazin, Nucl. Instrum. Methods B **204**, 174 (2003).
[32] F. Pűhlhofer, Nucl. Phys. A **280**, 267 (1977).
[33] National Nuclear Data Center, Brookhaven National Laboratory, Upton, NY.
[34] J. M. Freeman *et al.*, Rev. Phys. Appl. **12**, 1539 (1977).
[35] F. H. Ruddy and B. D. Pate, Nucl. Phys. A **127**, 305 (1969).
[36] L. F. Canto *et al.*, J. Phys. G **36**, 015109 (2009); Nucl. Phys. A **821**, 51 (2009).
[37] P. R. S. Gomes, J. Lubian, I. Padron, and R. M. Anjos, Phys. Rev. C **71**, 017601 (2005).
[38] L. C. Chamon, D. Pereira, M. S. Hussein, M. A. Candido Ribeiro, and D. Galetti, Phys. Rev. Lett. **79**, 5218 (1997).
[39] L. C. Chamon *et al.*, Phys. Rev. C **66**, 014610 (2002).